Transfer Functions to Measure Translational and Rotational Velocities with Continuous-Scan Laser Doppler Vibrometry

Shifei Yang
Graduate Research Assistant, Ph.D. Candidate
syang66@wisc.edu

&

Matthew S. Allen
Assistant Professor
msallen@engr.wisc.edu
Department of Engineering Physics
University of Wisconsin-Madison
535 Engineering Research Building
1500 Engineering Drive
Madison, WI 53706

Abstract

A laser Doppler vibrometer typically measures the translational velocity at a single point along the direction of incident light. However, it has been shown that rotational velocities can also be recovered by scanning the laser continuously along a line or circular path around that point. This work uses the harmonic transfer function concept, which is analogous to the transfer function in conventional modal analysis, to relate the measured rotational and translational velocities to the input force. With this concept, the continuous-scan approach can be combined with the conventional point by point scan approach, acquiring normalized translational and rotational velocities under various types of excitation conditions in the same amount of time that is required for obtaining only the translational velocity. The proposed approach is validated on measurements taken from a downhill ski under free-free boundary conditions. The influence of the circle size, the scanning rate and the surface quality on the noise level in the measured signal is discussed, and the measured deflection shapes using both the point and circular scan approaches are compared. Local slopes at measurement locations are computed from the identified principal rotational velocities, laying the foundation for constructing a much more accurate estimate of the deformation shape, which may be valuable in damage detection and/or model updating.

Keywords: modal testing, damage detection, laser Doppler vibrometer, rotational velocity, slope

1 Introduction

Continuous-Scan Laser Doppler Vibrometry (CSLDV) is a novel method of employing a laser vibrometer in which the laser spot sweeps over a structure continuously while capturing responses from a moving measurement point. The method can greatly accelerate the modal testing of structures with low frequency modes, which require long time records at every single measurement point when the conventional point by point scanning method is used. One can also obtain measurements with greatly increased spatial detail along the scan path, which is valuable in model correlation and updating [1], structural health monitoring, and damage detection.

A few algorithms have been devised to process measurements from CSLDV under various excitation conditions. Ewins group at Imperial College treats the operational deflection shape of a structure as a polynomial function of the moving laser position [2-6]. The coefficients of that polynomial are then obtained by transforming the amplitudes of the harmonics that are separated by the scanning frequency in the measured spectrum. Allen et al later presented a 'discrete' lifting approach [7, 8] that groups the measured responses at the same location along the laser scan path. The lifted measurements appear to be from a set of pseudo sensors but with a constant time delay between each other. The lifted spectra hence have only one peak for each mode, which allows conventional modal analysis curve fitting methods to be applied. Recently, algorithms based on linear time periodic system identification theory were used to process CSLDV measurements [9, 10]. When the laser scans a closed periodic pattern, measurements from CSLDV appear to be periodic. The harmonic transfer function of periodic systems allows natural frequencies, damping ratios and mode shapes to be extracted and compared under a variety of excitation conditions.

All these algorithms emphasize detecting translational deflection over an area on the structure, but the laser vibrometer can also be used to measure the rotational velocities over a small region. Ewins proposed a continuous scanning procedure to measure the translational as well as the angular vibration simultaneously [11]. He has proved that by scanning a line or a circle around the point of interest on a structure under sinusoidal input, the translational and rotational velocities are related to the central harmonic and its two sidebands in the measured spectrum. He then validated this procedure under a sinusoidal and a narrow-band random input. Recently, this procedure was adopted by Salman et al to reconstruct the operational vibration shape of a human hand using a line scan [12].

To compute the mobility and sideband frequency response functions, the forcing signal along with the product of the forcing signal and mirror driving signal were used as a reference in [11]. This work aims to develop an alternative algorithm based on the harmonic transfer function that allows us to extract velocity information using virtually any type of input, e.g. an impulse, random or swept-sine input. The harmonic transfer function is an extension of a frequency response function to linear time periodic systems [13-15]. With the harmonic transfer function, measurements from a circular scan can be processed as in conventional linear time invariant modal analysis, which allows windowing and averaging to reduce leakage and random noise. Also, the acquired translational and rotational velocities at multiple points can be easily stitched together to create mode shapes of the underlying structure. Hence, CSLDV can be combined with conventional point by point SLDV, measuring both translational and rotational velocities under various types of excitation conditions in the same amount of time that is required by SLDV to measure only 1-D translational velocity.

The rotational velocity at each measurement location represents the local slope of the vibration shape. Therefore, this rotational velocity information could be very useful in computing the local curvature that is valuable in damage detection applications [16, 17]. Conventionally, curvature is computed by a successive spatial differentiation of the deflection shape. The limitation is mainly dictated by a limited spatial resolution and the high frequency noise incurred by the second order differentiation. Using the additional local slope information at each measurement location, the deflection shape can be spline-fitted and hence a much more accurate curvature can be constructed. This paper investigates the noise in circular scan and shows how to identify the normalized translational and rotational velocities as well as the local slopes from the measured spectra, laying the foundation for computing the curvature shapes, which will be explored in detail in the next stage of this work.

The rest of this paper is organized as follows. Section 2 reviews the harmonic transfer function concept with particular emphasis on how to interpret the response spectra of a continuous scan measurement. In Section 3, the proposed technique is demonstrated on a downhill ski and the influence of circle size and scan frequency on laser noise level is discussed. In Section 4, the circular scan approach is used to identify the deflection mode shapes of the ski. The results are compared with those from a conventional point by point scan LDV. In Section 5, rotational velocities as well as the local slopes are obtained. Sections 6 summarizes this work.

2 Theoretical basis

This paper makes use of the harmonic transfer function concept that relates the output of a linear time periodic system to its input [18]. A detailed derivation of the harmonic transfer function for a general linear time periodic system can be found in the appendix. This section shows the simplified expression of the harmonic transfer function for CSLDV, proving that rotational velocities can be obtained from the measured spectrum.

2.1 Periodic model of CSLDV measurement

An N degree of freedom linear time invariant structure can be modeled using the well-known state space form with constant coefficients [19],

$$\begin{aligned} \dot{x} &= Ax + Bu \\ y &= Cx + Du \end{aligned} \tag{1}$$

Here x is internal state vector, u is the input and y is the output. A is the system matrix of the state space model, and B is the input matrix. When a laser Doppler vibrometer is employed to measure this invariant system, the output matrix C can be taken as a zero row vector with a one entry at the location the laser is measuring, e.g., if the laser is pointed at the k^{th} degree of freedom, then

$$C = \left[\underbrace{0 \ \cdots \ 0}_{N} \middle| \underbrace{0 \ \cdots \ 0 \ \overset{k}{1} \ 0 \ 0 \ \cdots \ 0}_{N} \right]_{1\times 2N} \tag{2}$$

Therefore, when the laser moves along a closed periodic pattern, the output matrix becomes periodic, $C(t)=C(t+T_A)$, where $T_A=2\pi/\omega_A$ is called the fundamental period. In addition, since only velocity information is picked up by the laser, the direct input matrix *D* is zero in the state space model.

One can diagonalize the state space equations by defining $x=Pq$, where *q* is the vector of modal participation factors, and

$$P=\begin{bmatrix}\Psi & \Psi^* \\ \Psi\Lambda & \Psi^*\Lambda^*\end{bmatrix} \tag{3}$$

is the diagonalizer of the state matrix *A*. Ψ is an *N*×*N* mode shape matrix that contains the modes of the system in its columns, $\Psi=\begin{bmatrix}\psi_1 & \cdots & \psi_N\end{bmatrix}$. The notation $()^*$ represents the complex conjugate. Λ is a diagonal matrix of the eigenvalues, $\lambda_r=-\zeta_r\omega_r+\mathrm{j}\omega_r\sqrt{1-\zeta_r^{\,2}}$ in terms of the *r*th natural frequency ω_r and damping ratio ζ_r.

Substituting $x=Pq$ into Eq. (1) and pre-multiplying the first equation by P^{-1}, one obtains the following uncoupled equations,

$$\begin{aligned}\dot{q}&=\Lambda q+P^{-1}Bu\\ y&=C(t)Pq\end{aligned} \tag{4}$$

The measurement point is continuously moving, therefore $C(t)P$ is a periodic 1×2*N* row vector of complex mode shapes,

$$C(t)P=\begin{bmatrix}C(t)\psi_1\lambda_1 & \cdots & C(t)\psi_N\lambda_N & C(t)\psi_1^*\lambda_1^* & \cdots & C(t)\psi_N^*\lambda_N^*\end{bmatrix} \tag{5}$$

The *r*th observed mode shape $C(t)\psi_r$ appears to be time periodic only because the position of the measurement point is periodic.

Eq. (4) in conjunction with Eq. (5) reveals that a linear time invariant structure measured by continuous scan laser Doppler vibrometry can be modeled as a linear time periodic system when a periodic scan pattern is used. The state space equations have constant matrices *A* and *B* since the underlying structure is linear time invariant. The only periodic term is the output matrix *C*. Hence, periodic system identification theory can be used to identify the natural frequencies, damping ratios, and mode shapes of the underlying time invariant structure measured by CSLDV.

2.2 Harmonic transfer function of CSLDV

This section shows the simplified derivation of harmonic transfer function specifically for CSLDV. The derivation for a general linear time periodic system can be found in the appendix. The derivation makes use of the general solution of a linear system with time varying coefficients [19],

$$y(t)=C(t)\Phi(t,t_0)x(t_0)+\int_{t_0}^{t}C(t)\Phi(t,\tau)B(\tau)u(\tau)d\tau+D(t)u(t) \tag{6}$$

Since the transfer function relates the steady-state response of a system to its input, the transient response term that includes the initial state $x(t_0)$ can be neglected. As was discussed in previous section, in CSLDV measurement the input matrix B is constant, and the direct input matrix D is zero. Eq. (6) then becomes,

$$y(t) = \int C(t)\Phi(t,\tau)Bu(\tau)d\tau \tag{7}$$

Here $\Phi(t,t_0)$ is called the state transition matrix. It relates the system state $x(t)$ at any time to the initial state $x(t_0)$ by,

$$x(t) = \Phi(t,t_0)x(t_0) \tag{8}$$

For a linear time invariant system with constant coefficients, the state transient matrix can be obtained directly as $\Phi(t,t_0) = e^{A(t-t_0)}$ [19], which can be further simplified as,

$$\Phi(t,t_0) = \sum_{r=1}^{2N} \psi_r L_r^T e^{\lambda_r (t-t_0)} \tag{9}$$

where ψ_r is the r^{th} mode vector of the underlying linear time invariant system, and L_r is the r^{th} column of $\Psi = \begin{bmatrix} \psi_1 & \psi_2 & \cdots \end{bmatrix}^{-T}$. Substituting Eq. (9) into the general solution of the state space model in Eq. (7), the measured velocity $y(t)$ by CSLDV becomes,

$$y(t) = \sum_{r=1}^{2N} C(t)\psi_r e^{\lambda_r t} \int L_r^T Bu(\tau)e^{-\lambda_r \tau} d\tau \tag{10}$$

$C(t)$ is a matrix of ones and zeros indicating which of the states are being measured by the laser. Since the observed mode shape $C(t)\psi_r$ is periodic on a periodic scan path, it is convenient to expand it in a Fourier series.

$$C(t)\psi_r = \sum_{n=-\infty}^{\infty} \bar{C}_{r,n} e^{\mathrm{i}n\omega_A t} \tag{11}$$

where $\bar{C}_{r,n}$ is the n^{th} Fourier coefficient of the r^{th} observed mode vector, $C(t)\psi_r$. Defining the constant $L_r^T B = \bar{B}_r$, Eq. (10) then becomes:

$$y(t) = \sum_{r=1}^{2N} \sum_{n=-\infty}^{\infty} \bar{C}_{r,n} e^{(\lambda_r + \mathrm{i}n\omega_A)t} \int \bar{B}_r e^{-\lambda_r \tau} u(\tau) d\tau \tag{12}$$

The above equation is the modal summation form of the measured velocity by CSLDV. It contains the frequency component at λ_r and its infinite number of harmonics each separated by the fundamental frequency ω_A. Wereley extends the concept of a transfer function for time invariant systems to time periodic systems by defining the Exponentially Modulated Periodic (EMP) signal [13]. This modulated signal is the summation of signals separated by multitudes of the fundamental frequency ω_A, hence a modulated input to a linear time periodic system causes a modulated output at the same collection of frequencies. In CSLDV measurements, the input $u(t)$ is time invariant but the output $y(t)$ is periodic due to the moving measurement point, hence,

$$u(t) = U_0 e^{\mathrm{i}\omega t} \quad , \quad y(t) = \sum_{n=-\infty}^{\infty} Y_n e^{(\mathrm{i}\omega + \mathrm{i}n\omega_A)t} \tag{13}$$

The harmonic transfer function can be derived by substituting the above expression into Eq. (12),

$$\sum_{n=-\infty}^{\infty} Y_n e^{(\mathrm{i}\omega + \mathrm{i}n\omega_A)t} = \sum_{r=1}^{2N} \sum_{n=-\infty}^{\infty} \bar{C}_{r,n} e^{(\lambda_r + \mathrm{i}n\omega_A)t} \int \bar{B}_r U_0 e^{(\mathrm{i}\omega - \lambda_r)\tau} d\tau \tag{14}$$

The summation can be further simplified after the integration, as follows,

$$\sum_{n=-\infty}^{\infty} Y_n e^{(\mathrm{i}\omega + \mathrm{i}n\omega_A)t} = \sum_{r=1}^{2N} \sum_{n=-\infty}^{\infty} \frac{\bar{C}_{r,n} \bar{B}_r}{\mathrm{i}\omega - \lambda_r} U_0 e^{(\mathrm{i}\omega + \mathrm{i}n\omega_A)t} \tag{15}$$

A harmonic balance approach can be used to match the terms with the same order of $e^{(\mathrm{i}\omega + \mathrm{i}n\omega_A)t}$,

$$Y_n = \sum_{r=1}^{2N} \frac{\bar{C}_{r,n} \bar{B}_r}{\mathrm{i}\omega - \lambda_r} U_0 \quad n \in (-\infty, \infty) \tag{16}$$

One can then define the exponentially modulated periodic signals in the frequency domain for CSLDV,

$$\begin{aligned} \mathbf{Y}(\omega) &= \begin{bmatrix} \cdots & Y_{-1}(\omega)^T & Y_0(\omega)^T & Y_1(\omega)^T & \cdots \end{bmatrix}^{\mathrm{T}} \\ \mathbf{U}(\omega) &= U_0(\omega) \end{aligned} \tag{17}$$

Hence, a transfer function is established in terms of the modal parameters of the state transition matrix, denoted by the harmonic transfer function.

$$\mathbf{Y}(\omega) = \mathbf{G}(\omega)\mathbf{U}(\omega) \tag{18}$$

Where,

$$\begin{aligned} \mathbf{G}(\omega) &= \sum_{r=1}^{2N} \frac{\bar{\mathbf{C}}_r \bar{B}_r}{\mathrm{i}\omega - \lambda_r} \\ \bar{\mathbf{C}}_r &= \begin{bmatrix} \cdots & \bar{C}_{r,-1} & \bar{C}_{r,0} & \bar{C}_{r,1} & \cdots \end{bmatrix}^T \end{aligned} \tag{19}$$

An H1 estimator is used to experimentally estimate the harmonic transfer function, since the noise is mostly from the speckle noise in the laser signal.

$$\mathbf{G}(\omega) = \frac{E(\mathbf{Y}(\omega) U_0^H(\omega))}{E(U_0(\omega) U_0^H(\omega))} \tag{20}$$

here $E()$ indicates the expected value. One should note that for a general linear time periodic system, the denominator would be a matrix of cross power spectrum of the modulated inputs. Therefore, one must have at least several averages for the spectrum matrix to be invertible.

2.3 Measuring rotational velocities

Figure 1 shows the scheme of employing CSLDV with a circular scan pattern to measure translational and rotational velocities of a local area. Assuming the standoff distance from the laser source to the point of interest is large compared to the scan radius *R*, the incident laser beam can be treated as perpendicular to the surface during the scan. Also, the deformation inside the circle can be neglected when *R* is reasonably small.

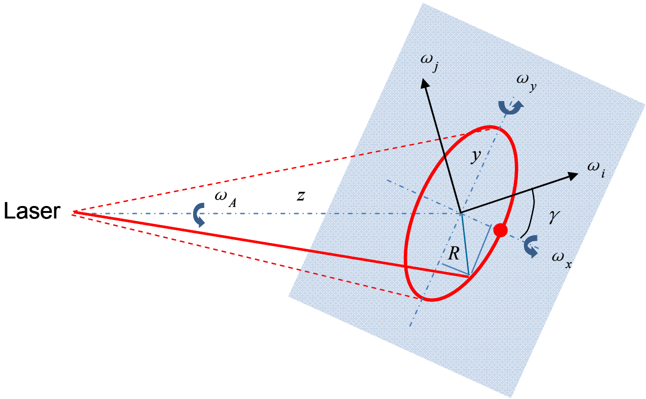

Figure 1: Scheme of measuring translational and rotational velocity using CSLDV

Ewins showed a similar derivation of the expression for the measured velocity in his work [11]. The sinusoidal angular vibration at a point on a surface can be decomposed into two orthogonal principal rotations that have a 90-degree phase difference,

$$\begin{aligned}\omega_i &= \Theta_A \cos(\omega t + \beta)\\ \omega_j &= \Theta_B \sin(\omega t + \beta)\end{aligned} \tag{21}$$

Θ_A and Θ_B are the amplitudes of the principal rotational velocities along i and j axis. β is the initial phase of the oscillation. Note that the in plane rotation ω_k is assumed to be zero.

Suppose the initial position of the laser is at the red dot on x axis and the laser scans counterclockwise with a constant speed of ω_A, the measured velocity $v(t)$ from a laser Doppler vibrometer contains three components: the translational velocity $v_z(t)$, the velocity component along the z axis introduced by the rotation $\omega_x(t)$, and the velocity component along the z axis introduced by the rotation $\omega_y(t)$.

$$v(t) = v_z(t) + \omega_y(t)x(t) + \omega_x(t)y(t) \tag{22}$$

$x(t)$ and $y(t)$ are the position of the laser spot with respect to a reference frame that is fixed in the space. The orientation of the principal rotational velocities with respect to this reference frame is not known ahead, and this orientation may vary from point to point. However, if we assumed this angle to be γ, the rotational velocities along the x and y axis can be obtained via a rotation matrix, as

$$\begin{aligned}\omega_x &= \omega_i \cos(\gamma) - \omega_j \sin(\gamma) \\ \omega_y &= \omega_i \sin(\gamma) + \omega_j \cos(\gamma)\end{aligned} \tag{23}$$

The laser position at any time instant is

$$x(t) = R\cos(\omega_A t), \qquad y(t) = R\sin(\omega_A t) \tag{24}$$

Notice that when the structure is under sinusoidal excitation, the translational can be written as

$$V_z(t) = Z\cos(\omega t + \alpha) \tag{25}$$

where Z is the amplitude of the translational velocity, and α is the initial phase of oscillation. Substituting Eq. (21), (23), (24) and (25) into Eq. (22), and then simplifying Eq. (22) using trigonometric functions, yields

$$v(t) = Z\cos(\omega t + \alpha) + R\frac{\Theta_B + \Theta_A}{2}\sin((\omega + \omega_A)t + \beta + \gamma) + R\frac{\Theta_B - \Theta_A}{2}\sin((\omega - \omega_A)t + \beta - \gamma) \tag{26}$$

The measured velocity signal using CSLDV will include all the translational and rotational velocities at the point of interest. For example, Figure 2 shows the measured spectrum when the laser scans at 150Hz on a beam that was excited at its first mode at 13Hz. The translational velocity and its phase can be obtained from the peak at 13Hz, and the rotational velocities can be recovered from the two peaks at 137Hz and 163Hz according to Eq. (26).

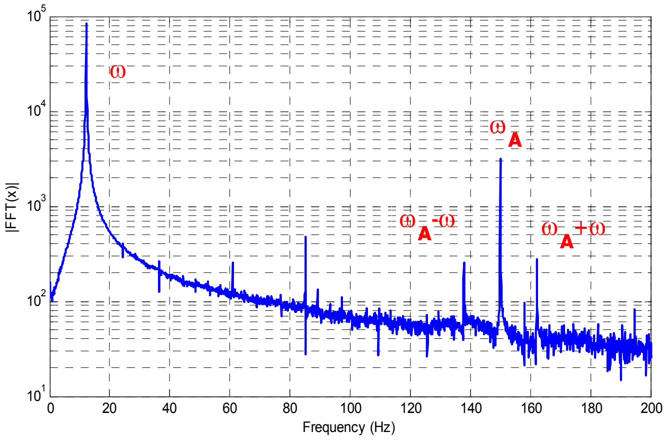

Figure 2: Spectrum of measured CSLDV signal with a 150Hz scan frequency

To compute the harmonic transfer function from a circular scan measurement, the measured velocity will be exponentially modulated according to Eq. (13). One should note that the modulation is essentially a process of making frequency shifted copies of the measured spectrum by nω_A in the frequency domain. Therefore, the translational velocity at ω corresponds to the Y_0 term, and the rotational velocities at the frequency lines of ω_A-ω and ω_A+ω can be related to the Y_{-1} and Y_1 term in Eq. (17). This allows us to use conventional curve fitting tools for time invariant systems to interpret measurements from the circular scan under any type of input. Additionally, since the transfer function is computed, the acquired translational and rotational velocities at multiple points can be easily stitched together to create mode shapes of the underlying structure.

2.4 Computing curvature

The curvature of a surface is proportional to the surface strain, therefore is very sensitive to cracks and subsurface damages [16]. The change in curvature has been used widely as the indicator of potential damage in structures. Conventionally, to compute the curvature, shapes at several measurement locations have to be patched together and then a second order finite difference is computed. Figure 3 shows an example of computing the curvature from an experimentally measured deflection mode shape. The circles represent sensor locations. To obtain the curvature c_i at the i^{th} point, a finite difference approximation can be used, as follows,

$$c_i = \frac{(y_{i+1} - y_i) - (y_i - y_{i-1})}{h^2} \tag{27}$$

Here y_{i} is the deflection at the i^{th} point, and h is the step size between two neighboring sensors. This method is usually limited by the availability of a dense measurement gird. In addition, the measurement noise in deflection mode shapes is amplified by the second order derivative.

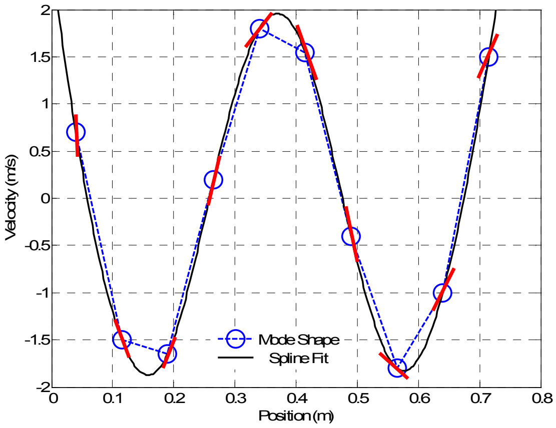

Figure 3: Scheme of constructing curvature using translational velocity

On the other hand, the point by point scan laser Doppler vibrometry allows spatially detailed mode shapes to be extracted in a short time. The derivation in Section 2.3 shows that by combining the circular scan approach with the point by point scanning LDV, the translational velocity as well as the principal rotational velocities can be measured in the same amount of time that is required to measure only the translational velocities. This is extremely beneficial for computing curvature since the amplitudes of rotational velocities at any measurement location correspond to the local slope of the vibration shape, as demonstrated by the short red line in Figure 3. Therefore, the deflection shape together with the local slopes can be used to construct an accurate spline-fit to the deflection that could greatly reduce the error in the computed curvature shapes. With the harmonic transfer function concept, curvature shapes in a measurement grid can be patched and used to characterize the damages in the underlying time invariant system.

As discussed earlier, the major focus of this work is to obtain the defection mode shapes and local slopes from circular scan measurement. In next stage, these deflection and slope information will be used to construct 1D and 2D curvature shape of the underlying structure.

3 Experimental setup and speckle noise

The experimental validation of the proposed circular scan algorithm was performed on a downhill ski, which is a complex structure formed by laminating several materials together and hence can be very challenging to model accurately. As shown in Figure 4 (a), the ski was hung using two soft bungee cords to simulate free-free boundary conditions. A shaker with a function generator was used to excite the ski. A load cell was installed on the tip of the stinger to measure the input force applied to the ski shown in Figure 4 (b). A Polytec PSV-400 (633nm laser) vibrometer with an external x-y mirror system [10] was used to measure the surface velocity at a standoff distance of approximately 2.5m. The scanner works in a closed loop, and each mirror is fitted with a position detector that measures the angle of the scanner, which allows very precise control of the laser position.

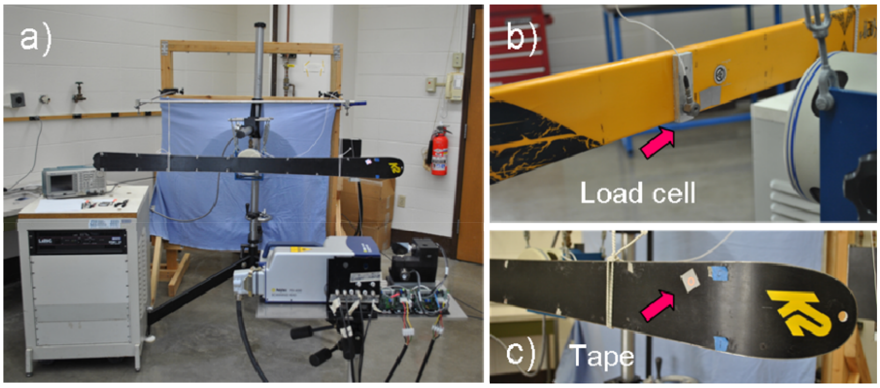

Figure 4: Experimental set up. a) Testing scheme, b) Load cell, c) Retro-reflective tape

In this section, the speckle noise associated with the circular scan approach is investigated. Laser speckle is formed when coherent light scatters and interferes from an optically rough surface. Speckle noise has been studied extensively prior to this work [20-25]. The effect of focus size, target surface roughness, scan speed and standoff distance etc. has been investigated, and even a simulated model has been created. The purpose of this section is not to challenge the well-established model but to survey the influence of scan frequency, circle size and the surface quality of the ski on the noise level in the measurements, such that a set of optimal experimental parameters can be selected for the following tests.

The scan frequencies tested were 20Hz up to 300Hz with a 20Hz step size. The nonlinearity of the mechanical system is considered to be dominant when the mirror system scans at a higher frequency. The scan circle diameters tested were from 1/16in to 8/16in with a step size of 1/16in. When the circle size is larger than 8/16in, higher order harmonics of each mode tend to appear in the measurement spectrum, indicating that mode shapes along the circle path are being measured. Also, one should note that the maximum circle size may vary for different structures and different modes because of the assumption that deformation inside of the circle shall be neglected. In addition to the circular scan, conventional tests where the laser was pointed at a stationary point were conducted as a reference. Tests were repeated on three different surfaces, namely, the black bottom of the ski (Figure 4 (a)), the yellow top of the ski (Figure 4 (b)) and 3M retro-reflective tape (Figure 4 (c)).

Figure 5 shows the measured spectrum on the black bottom surface when the laser scanned at the frequency of 40Hz and the circle size was 5/16in. The ski was excited at its first natural frequency of 19Hz. The test duration was 15 seconds with a sampling frequency of 10,240Hz. To estimate the noise level, a linear mode was fit to the dominant peak in the spectrum using the algorithm of mode isolation [26]. This linear mode (green line) was then subtracted from the measured spectrum (grey line) and the residue (red line) was considered as the noise. Then the noise signal in the frequency domain was transformed via an inverse fast Fourier transform to the time domain, where the mean value and the standard deviation of the noise were calculated.

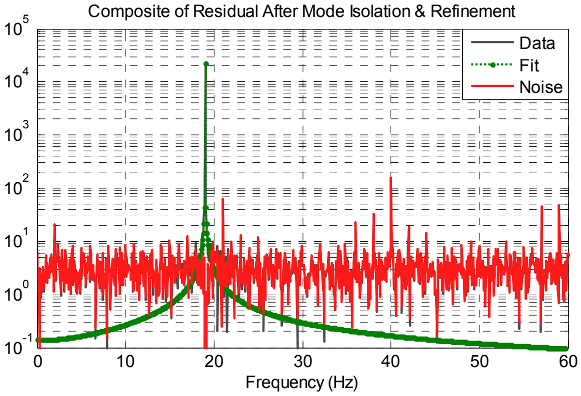

Figure 5: Measured spectrum with 40Hz scan frequency and 5/16in circle size

Figure 6 shows the mean and the standard deviation of the noise when the laser scans on the retro-reflective tape. The dashed red horizontal lines in both plots represent the value from the stationary point test. It can be found that the noise is smallest when the laser is pointed at a stationary point on the tape. The tape is coated with micro-scale glass beads that reflect most of the light in a concentrated cone back to the detector [27]. Therefore the speckle noise is minimized. When the laser is scanning around a circle, the noise level as well as the standard deviation increase with the scan frequency and the circle size. This phenomenon agrees with what was found in a previous work [25]. When the ski is excited at its first natural frequency, the motion of the ski is a combination of translational, rotational, as well as the in-plane rigid body motion due to the misalignment of the shaker, meaning the speckle pattern exhibits both ‘translation’ and ‘evolution’ changes [22]. When the laser scans on a periodic path, the measured speckle noise contains mostly periodic components. The magnitude of this periodic noise increases severely with surface velocity, which is the product of the scan frequency and the perimeter of the scan circle.

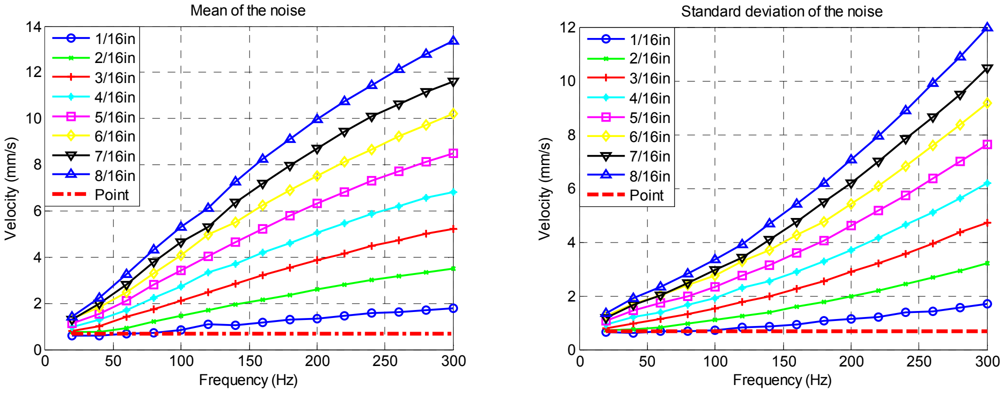

Figure 6 Noise level on retro-reflective tape

Figure 7 shows the mean and the standard deviation of the noise when scanning on the dark bottom surface of the ski. The noise pattern is similar to what was observed on the retro-reflective tape. However, the mean of the noise at a stationary point is higher than some of the circular scan results, and the standard deviation at a stationary point is much higher. When the laser hits a stationary point on a rough surface, the light is scattered to all directions randomly and only a small portion can travel back to the detector. The laser could be located at a point where the light is dominated by a dark speckle, as is often happened in conventional point by point scanning LDV. This may cause a dramatic change in noise level that partially explains the jagged nature of the noise level when the circle size is 1/16in. In contrast, when the circular scan approach is adopted with appropriate circle size, the signal level is likely to be large over some portion on the circle path, and the total noise level is reduced due to this ‘averaging’ effect. Therefore, in Figure 7 a decrease in the noise level and in the standard deviation is observed when the scan frequency is lower than 60Hz. After 60Hz, the periodic noise becomes dominant and the trend that was observed in Figure 6 appears.

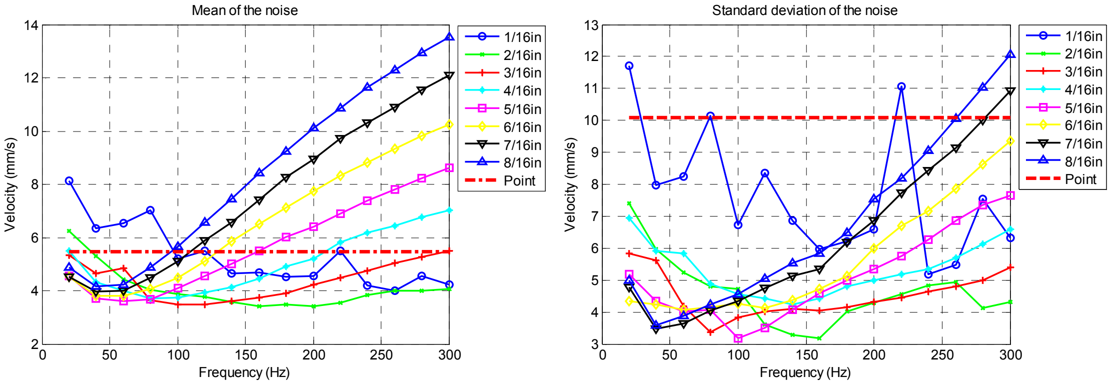

Figure 7: Noise on black bottom surface

As shown in Figure 8, the decrease in noise level becomes more obvious when the laser scans on the yellow top surface that is smoother than the dark bottom surface of the ski. Also notice that the noise and its deviation are much higher for the stationary laser on this surface. Insight into this result can be gained from previous studies on speckle noise and surface roughness [22, 27]. Scattering from smooth surfaces reduces the range of phase excursions in the laser. However, due to the mirror like behavior of the polished surface, the scattering angle is more likely to be unusable which leads to signal loss. For circular scan measurements, it is observed that when the scan frequency is smaller than 120Hz, the noise level as well as the standard deviation decrease with the increasing circle size and scan frequency. When the scan frequency is larger than 160Hz, the speckle noise and deviation increase with the scan frequency and the circle size, indicating a dominant periodic speckle pattern in this region. One should also note that the overall noise level on the smooth yellow top surface is larger than those from the dark bottom surface or the retro-reflective tape, perhaps due to the mirror like behavior.

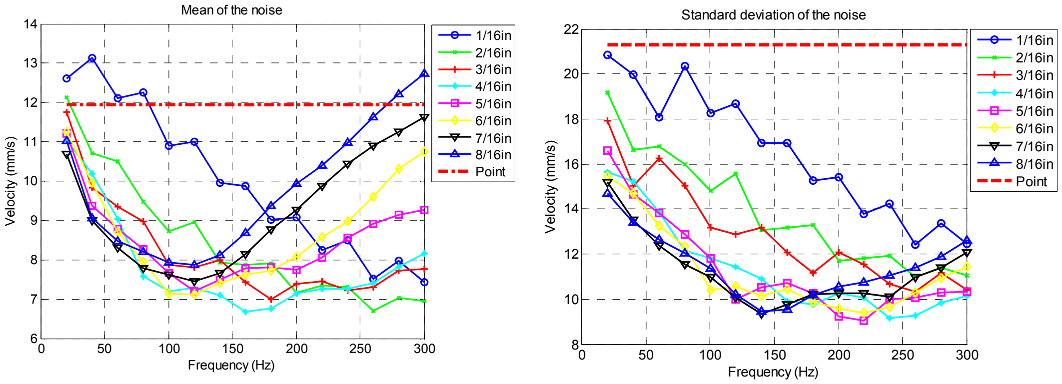

Figure 8 Noise on Yellow top surface

As indicated earlier, the purpose of this section is to help in selecting appropriate testing parameters that lead to a lower noise level in measured signal, which would improve the uncertainty in the measured translational and rotational velocities, and eventually lead to a more accurate curvature shape in the next stage. In the following section, a set of circular scan tests will be conducted to reconstruct the mode shapes of the ski using a swept-sine excitation. A scan frequency of 200Hz and a circle size of 5/16inch are selected to perform the tests so that noise is optimized on the black bottom surface of the ski that is under swept sine excitation up to 100Hz.

4 Deflection mode shapes

Prior to the circular scan test, a conventional hammer test with an accelerometer was performed to identify the natural frequencies of the ski under free-free boundary condition. A few frequencies at 1.5Hz 4.5Hz, 19Hz, 42Hz and 75Hz were identified. The modes at 1.5Hz and 4.5Hz were known to be the rigid body modes. The point by point scanning tests were then performed at the rest of the frequencies on the black bottom surface of the ski using the Polytec's software package. The laser scanned 3 lines all over the ski with 40 points along each line, as shown in Figure 9. At each point the test duration was 12 seconds. The ski was excited at its natural frequencies at 19Hz, 42Hz, 75Hz, as well as a coupling frequency between the ski and the shaker at 23.2Hz. The measured mode shapes are shown in Figure 9.

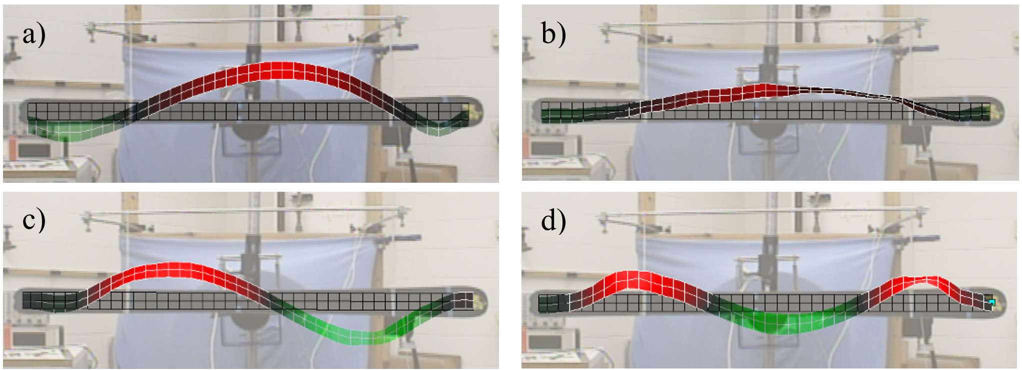

Figure 9: Measured mode shapes using scanning LDV. a) 1st bending mode at 19Hz, b) Coupling mode at 23.2Hz c) 2nd bending mode at 42Hz, d) 3rd bending mode at 75Hz

It is clear that the mode at 19Hz is the first bending mode of the ski (Figure 9 (a)), and the mode at 42Hz is the second bending mode (Figure 9 (c)). Note that the shaker is installed slight off the center of the ski to better excite the second bending mode. The mode at 75Hz is found to be the third bending mode (Figure 9 (d)). There is also a coupling mode between the shaker and the ski at 23.2Hz. Its mode shape is show in Figure 7(b), which is a combination of bending and torsional motion. However, one issue noticed in all measured mode shapes is that the amplitudes of the vibration shapes are close to zero at both ends of the ski. This phenomenon is due to the large angle of the incidence laser with respect to the longitudinal direction of the ski such that the detector loses the signal, and the amplitudes of the shapes appear to be zero.

The conventional scanning LDV test provides the basic mode shape information about the ski. A linear swept-sine test was then performed on the dark bottom surface to validate the proposed algorithm based on the harmonic transfer function. The driving frequency of the shaker is from 30Hz to 100Hz so as to avoid the coupling mode at 23.2Hz that may damage the shaker. Therefore, only the second and third bending modes are well excited using this swept-sine input. The sweep time is 15 seconds from 30Hz to 100Hz and 15 seconds for the return. Limited by the angle of the mirror, only half of the ski was tested, with 2 lines all over the ski and 28 measurement points along each line. The total test duration at each point is 200 seconds.

Figure 10 shows the measured mass-normalized mode shapes using the point by point scan approach and the circular scan approach, while all other testing parameters including the standoff distance and point locations were kept identical. The identified second and third bending mode shapes agree well with the corresponding shapes from the scanning LDV test in Figure 9. However, it is obvious that the mode shapes from circular scan test are much smoother than those from the point by point test. The reason for this difference is that the circular scan approach can provide better signal to noise ratio on a rough surface when appropriate scanning frequency and circle size are selected, as discussed in detail in Section 3. When the laser was scanning a circle around the point at x=0.5m from the driving point on the ski, part of the circle path landed on the bungee cord. This explains the error of the second bending mode shape that is observed near x=0.5m in Figure 10 (b). Nevertheless, the mode shape at this location is still relatively clean compared to the shape at the same location from the point by point test. This characteristic of circular scan approach is extremely important in computing curvature shapes, which is vulnerable to the noise in the measured deflection shapes because of the second order differentiation [16].

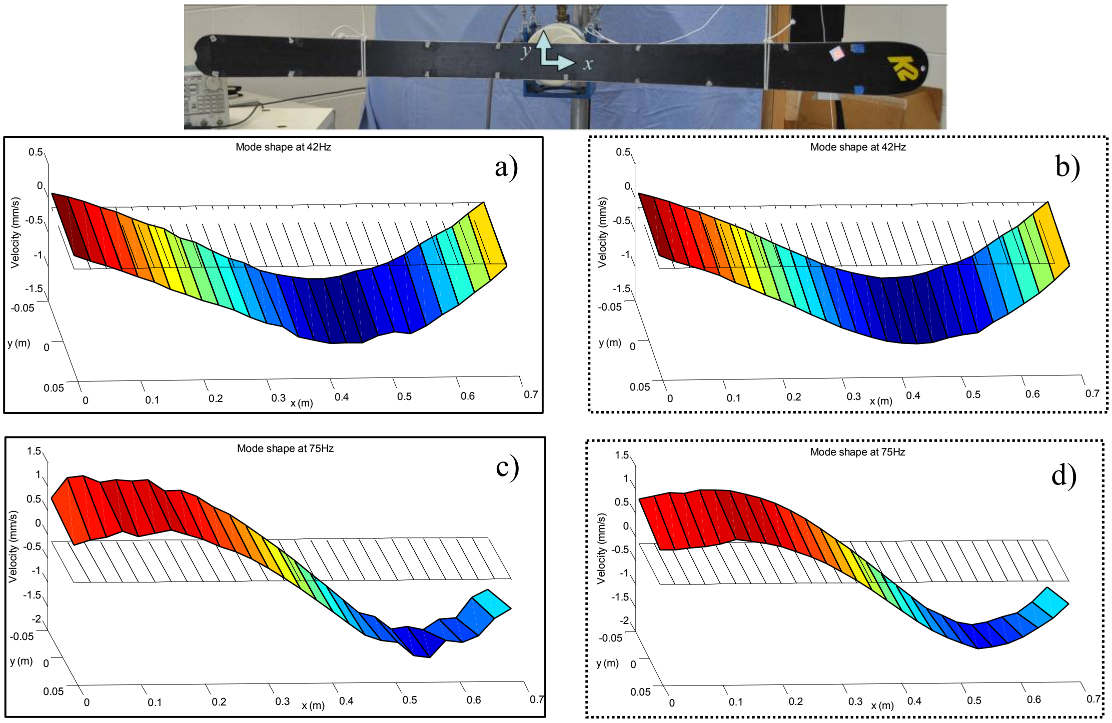

Figure 10: Measured mode shapes a) Mode at 42Hz by point measurement, b) Mode at 42Hz by circular scan, c) Mode at 75Hz by point measurement, d) Mode at 75Hz by circular scan

5 Rotational velocity and local slope

Besides the advantages in measuring translational velocity, the circular scan approach can also be used to simultaneously measure the principal rotational velocities, as was proved in Section 2.3. This section makes use of the harmonic transfer function of linear time periodic systems to interpret measurements from the circular scan approach and to compute the translational and rotational velocities. The local slopes at each measurement location are then transformed from the principal rotational velocities.

To estimate the harmonic transfer function that relates the measured velocities to the input force, n= -2:2 is used to form the exponentially modulated output signals in Eq. (17). An accurate scanning frequency ω_A is critical in the modulating process because of the $e^{(i\omega+in\omega_A)t}$ term. The phase errors in the modulated signals accumulate with time for an inaccurate scan frequency, and eventually lead to unreliable output spectra. Therefore, a multi-sine signal is fitted to the recorded mirror output signal to find the accurate scanning frequency. It is found that when the mirror was driven at 200Hz, the actual scan frequency was at 200.0153Hz. The mirror signals, velocity signal and the input force are then resampled such that there are an integer number of measurement points along each scan cycle. For example, when the laser scans at 200.0153Hz, the resampled measurement has 26 points on each circle, as shown in Figure 11, where the red dots represent measurement locations after resampling.

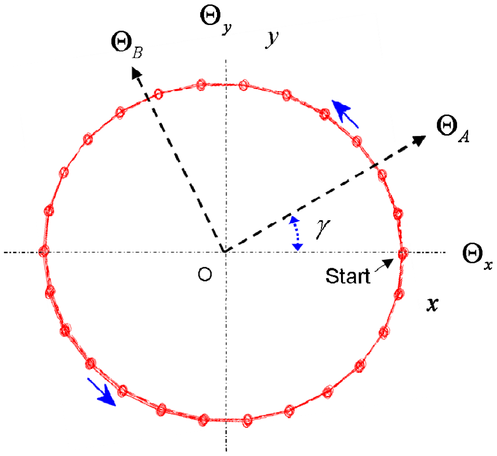

Figure 11 Circular scan after resampling

This resampling procedure is necessary in computing the harmonic transfer function since averaging is used to reduce the random noise. The input signal and modulated output signals are broken into 30 seconds sub-blocks with a 75% overlap between neighboring blocks, resulting in 23 sub-blocks over the 200 seconds time history. However, as seen in Figure 11, the measurement has to start at the same location on the scan cycle for each sub-block in order to maintain a constant angle γ between the starting point and the principal rotational velocities in Eq. (26). In this case, the auto spectra of the modulated output signals would have the synchronized phase with the input force over each block and no phase error will be incurred during the averaging. A Hanning window is then applied to each block to reduce the leakage. Since most of the noise is from the laser speckle, the H1 estimator in Eq. (20) is used to estimate the harmonic transfer function. Once the principal rotational velocities Θ_A and Θ_B of a mode are identified, the slope of the deflection shape along the x axis can be obtained by projecting the principal rotational velocities to the y direction using the angle γ, and similarly for the slope along the y axis. The angle γ can be obtained from the sidebands and may vary from point by point.

Figure 12 shows the computed harmonic transfer functions at the same location of the ski on the dark bottom surface and on the retro-reflective tape, respectively. The harmonic transfer function has the similar form as the transfer function of a single-input multiple-output linear time invariant system. However, the mode shapes at the natural frequency of 42Hz and 75Hz are no longer the physical deformation at each measurement location. Rather, they are related to the translational and rotational velocities at that point. Specifically, the amplitudes of $G_{-1,0}$ and $G_{1,0}$ are related to the principal rotational velocities and have much smaller amplitudes compared to the translational velocity at $G_{0,0}$. Here, $G_{i,0}$ represents the harmonic transfer function Y_i/U_0, which corresponds to the i^{th} line in Figure 12. Therefore, rotational velocities are more vulnerable than translational velocities to the speckle noise. Theoretically, according to Eq. (26), the amplitudes of $G_{-2,0}$ and $G_{2,0}$ should be either zero or very small compared to the value of $G_{-1,0}$ and $G_{1,0}$. However, this is not the case when the laser is scanning on the black bottom surface, as shown in Figure 12. The amplitudes of $G_{-1,0}$ and $G_{1,0}$ are close to those of $G_{-2,0}$ and $G_{2,0}$. This is because the overall speckle noise level is larger on black bottom surface than that on the retro-reflective tape.

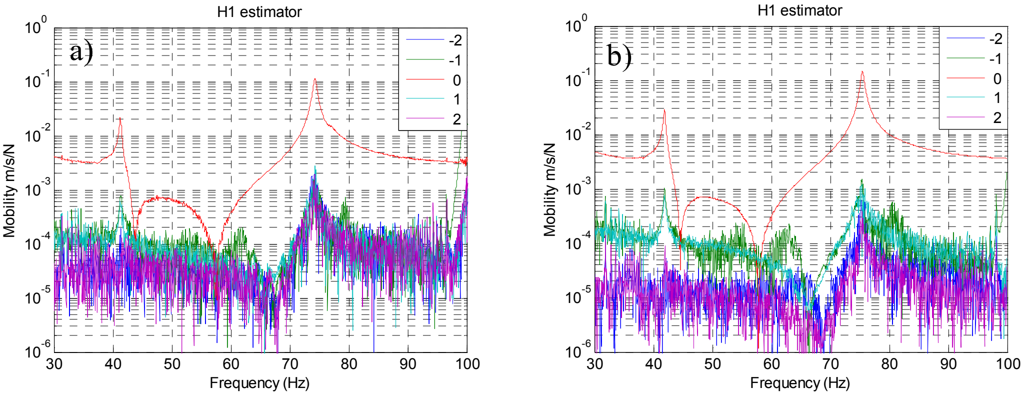

Figure 12 Harmonic transfer function of circular scan at the same point, a) on black bottom surface, b) on retro-reflective tape

To detect accurate rotational velocities and local slopes, the circular scan tests were performed on the retro-reflective tape, using a 4×10 measurement grid with a step size of 27mm in the longitudinal direction of the ski, and a step size of 23mm in the other direction. For consistency, other parameters remained the same as those in previous tests. Figure 13 shows the composite harmonic transfer function from a circular scan measurement at a single point on the tape. The harmonic transfer function is fitted with the algorithm of mode isolation [28]. It appears that the fitted modes reduce the harmonic transfer function very well. The identified amplitudes and phase for the second and third bending mode are listed in Table 1. Notice that the amplitudes of $G_{-1,0}$ and $G_{1,0}$ terms are an order of magnitude smaller than that of the $G_{0,0}$ term, which corresponds to the translational velocity at that measurement location.

In any event, the rotational and translational velocities are computed according to Eq. (26), and the velocities are listed in Table 1 as well. It was found that for the second bending mode at 42Hz, the principal rotational velocity Θ_A is the dominant rotation at this measurement location. It has a magnitude of 0.3816rad/s/N and is orientated approximately 80 degrees from the longitudinal direction of the ski. The principal rotational velocity Θ_B has the magnitude of 0.0641 rad/s/N and is oriented 90 degrees from Θ_A. This result agrees with our experimental observation that the rotational motion associated with bending modes should be in the direction that is perpendicular to the longitudinal direction of the ski. The rotational velocities of the third bending mode at 75Hz are slightly nosier and have larger angle with respect to the longitudinal direction of the ski.

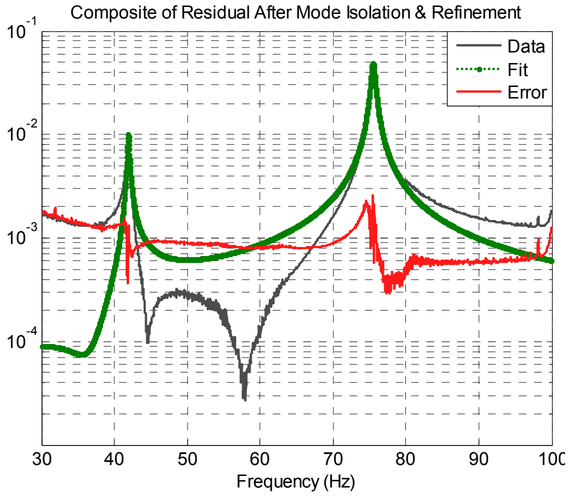

Figure 13 AMI fit of the harmonic transfer function

Table 1 Measured translational and rotational velocities from circular scan

Mode at 42Hz					
Mode shape	Amplitude mm/s/N	Phase angle (Degree)	Velocities	Amplitude	γ Angle(degree)
$G_{-1,0}$	0.9	16.0369	Θ_A	0.3816 rad/s/N	79.9076
$G_{0,0}$	26	-166.4050	Z	26 mm/s/N	/
$G_{1,0}$	0.6	-4.1478	Θ_B	0.0641 rad/s/N	169.9076
Mode 75Hz					
Mode shape	Amplitude mm/s/N s	Phase angle (Degree)	Velocities	Amplitude	γ Angle(degree)
$\bar{C}_{r,-1}$	22	25.7603	Θ_A	0.8053 rad/s/N	34.0818
$\bar{C}_{r,0}$	252.3	-0.5437	Z	252.3 mm/s/N	/
$\bar{C}_{r,1}$	10	-86.0761	Θ_B	0.2872 rad/s/N	124.0818

The above results are from the measurement at a single point. The translational and rotational velocities at all other points in the 4×10 measurement grid are computed in the same manner. Note that the orientations of principal rotational velocities are different from one point to another. However, the slopes of the second and the third bending mode can still be obtained since the angle γ for each mode can be recovered from the harmonic transfer function. The shapes of the second and third bending mode along the top line are plotted in Figure 14. The principal rotational velocities at each measurement location are projected to the y axis to compute the local slopes along the longitudinal direction of the ski, which are shown as red short lines in Figure 14. It is found that the curve of the second bending mode matches very well with the computed slopes from the rotational velocities. However, some errors are observed at the first few points in the third bending mode. This is perhaps due to the large amplitudes of $G_{-2,0}$ and $G_{2,0}$ as seen Figure 12 (b). The circle size could be too large for the second mode in this region of the ski such that the laser picked up some higher order harmonics along the circle, and the principal rotational velocities were not accurately estimated.

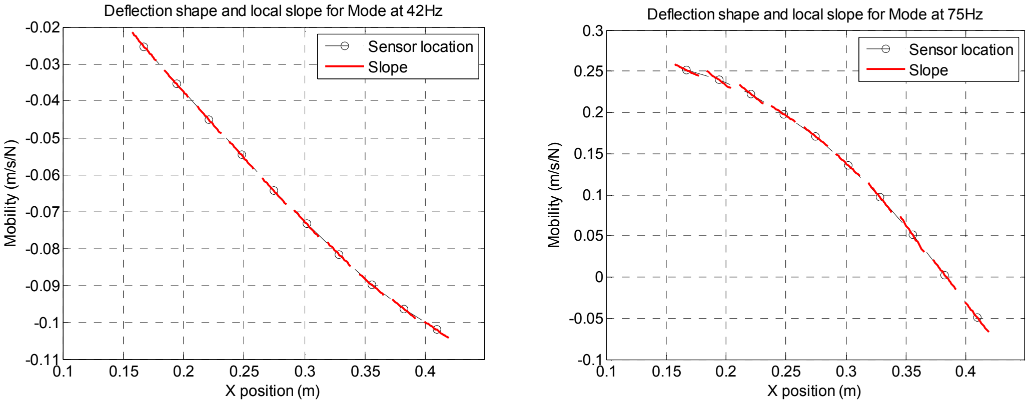

Figure 14 Measured deflection shape and local slope using the circular scan approach

Table 2 compares the computed slopes using the projection of rotational velocities and the computational slopes obtained via a forward finite difference. We can see that the slopes of the second bending mode from both methods agree very small, while the slopes at the first few points of the third bending mode have slightly larger error .

Table 2 Computed slopes and the forward difference results

		P1	P2	P3	P4	P5	P6	P7	P8	P9	P10
Mode 2 at 42Hz	Slope	-0.3864	-0.3640	-0.3744	-0.3751	-0.3550	-0.3616	-0.3290	-0.2819	-0.2583	-0.2241
	Forward difference	-0.3762	-0.3606	-0.3542	-0.3608	-0.3275	-0.3082	-0.3031	-0.2466	-0.2075	/
Mode 3 at 75Hz	Slope	-0.6844	-1.0661	-1.1556	-0.9592	-1.2232	-1.3595	-1.7794	-2.1631	-1.8609	-1.8418
	Forward difference	-0.4376	-0.6410	-0.8893	-1.0155	-1.2874	-1.4569	-1.6708	-1.8003	-1.9127	/

Figure 15 shows the orientations and amplitudes of principal rotational velocities at all the measurement points for the second bending mode at 42Hz, with the length of the arrow scales to the amplitude of a rotational velocity. It can be seen that the orientations and amplitudes of principal rotational velocities are consistent at most points. Figure 14 together with Figure 15 can be used to compute a 1-D or 2-D spline-fit to the deformation shape, which can be used to compute a much more accurate curvature for damage detection. This part will be explored in the next stage of this work.

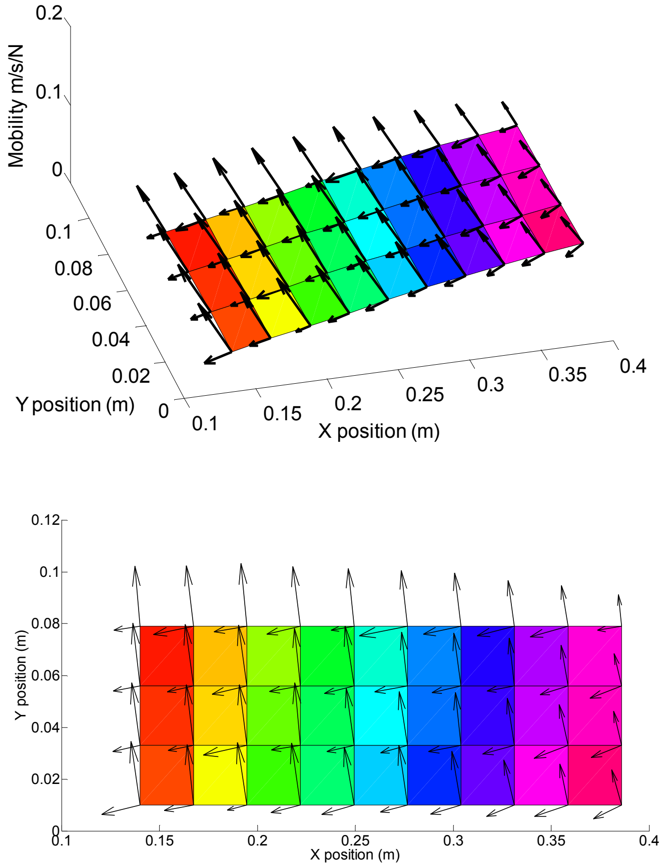

Figure 15 Translational and rotational velocities for the first mode

6 Conclusion

Signals measured using continuous scan laser Doppler vibrometry can be represented as the output of a linear time periodic system when a closed, periodic scan pattern is used. This work proposed a new algorithm based on the harmonic transfer function of linear time periodic system to process measurements from a circular scan approach, allowing the translational and rotational velocities to be extracted simultaneously. Using this new approach, the circular scan approach can be combined with the conventional point by point scan approach, acquiring translational and rotational velocities at each point in a measurement grid in the same amount of time that is required for obtaining only the translational velocity. Also, because the method is based on a transfer function description, virtually any desired input can be applied.

The proposed algorithm was validated on a downhill ski under free-free boundary conditions. The ski is a complex structure that can be very challenging to model accurately. This work studied the influence of the scanning rate, circle size, and surface quality on the noise level in measured signal. The results showed that in some situations the circle scan approach can provide a lower noise level and standard deviation than the conventional point approach, if the scan frequency and circle size are chosen appropriately. It seems that by scanning in a circle one can avoid the possibility of the detector area being dominated by a dark speckle, or by a region where speckle noise is especially severe, and thus reduces the speckle noise and the potential for signal dropouts. On the other hand, the circle scan increases the noise if the radius of the scan and/or the scan frequency are too large.

The circular scan approach was then applied over a grid of circles (points) to measure the mode shapes on the black bottom surface of the ski. A 200Hz scan frequency and a 5/16in circle size were selected based on the previous study. The circular scan approach was found to provide smoother and more reliable mode shapes than the conventional point by point approach in this scenario.

The harmonic transfer function concept was also used to extract the principal rotational velocities of the ski. The amplitudes of the rotational velocities were found to be much smaller than those of the translational velocities, and hence even though the circle scan provided a greater signal to noise ratio than the point scan, the noise was still too large to accurately measure surface rotation. However, retro-reflective tape was applied to the surface and found to reduce the noise so that the rotations could be accurately measured. Then the acquired rotational velocities were used to compute the slope of the mode shape at the measurement locations, the results were found to agree well with the trend of the shapes found by measuring the translational velocity, suggesting that the method is accurate. Future work will focus on computing a spline-fit to the surface shape using both the deflection and slope information, so that the curvature of the surface can be computed much more accurately.

Acknowledgements

The authors wish to thank the National Science Foundation for supporting this research under the Grant No. CMMI-0969224.

Reference

[1] M. S. Allen and D. M. Aguilar, "Model Validation of a Bolted Beam Using Spatially Detailed Mode Shapes Measured by Continuous-Scan Laser Doppler Vibrometry," presented at the 50th AIAA/ASME/ASCE/AHS/ASC Structures, Structural Dynamics, and Materials Conference, Palm Springs, California, 2009.

[2] C. W. Schwingshackl, A. B. Stanbridge, C. Zang, and D. J. Ewins, "Full-Field Vibration Measurement of Cylindrical Structures using a Continuous Scanning LDV Technique," presented at the 25th International Modal Analysis Confernce (IMAC XXV), Orlando, Florida, 2007.

[3] A. B. Stanbridge and D. J. Ewins, "Modal testing using a scanning laser Doppler vibrometer," *Mechanical Systems and Signal Processing,* vol. 13, pp. 255-70, 1999.

[4] A. B. Stanbridge, M. Martarelli, and D. J. Ewins, "Measuring area vibration mode shapes with a continuous-scan LDV," *Measurement,* vol. 35, pp. 181-9, 2004.

[5] M. Martarelli, "Exploiting the Laser Scanning Facility for Vibration Measurements," Ph.D. Ph.D., Imperial College of Science, Technology & Medicine, Imperial College, London, 2001.

[6] A. B. Stanbridge, A. Z. Khan, and D. J. Ewins, "Modal testing using impact excitation and a scanning LDV," *Shock and Vibration,* vol. 7, pp. 91-100, 2000.

[7] M. S. Allen, "Frequency-Domain Identification of Linear Time-Periodic Systems using LTI Techniques," *Journal of Computational and Nonlinear Dynamics* vol. 4, 24 Aug. 2009.

[8] S. Yang, M. W. Sracic, and M. S. Allen, "Two algorithms for mass normalizing mode shapes from impact excited continuous-scan laser Doppler vibrometry," *Journal of Vibration and Acoustics,* vol. 134, p. 021004, 2012.

[9] S. Yang and M. S. Allen, "Output-Only Modal Analysis Using Continuous-Scan Laser Doppler Vibrometry and Application to a 20kW Wind Turbine," *Mechanical Systems and Signal Processing,* vol. 31, August 2012 2011.

[10] S. Yang and M. S. Allen, "A Lifting Algorithm for Output-only Continuous Scan Laser Doppler Vibrometry," presented at the AIAA, Hawaii, 2012.

[11] A. B. Stanbridge and D. J. Ewins, "Measurement of translational and angular vibration using a scanning laser Doppler Vibrometer," *Vibration Measurement,* vol. 2358, pp. 37-47, 1994.

[12] M. Salman and K. G. Sabra, "Broadband measurement of translational and angular vibrations using a single continuously scanning laser Doppler vibrometer," *Journal of Acoustical Society of America,* vol. 132, pp. 1384-1391, 2012.

[13] N. M. Wereley, "Analysis and Control of Linear Periodically Time Varying Systems," PhD, Department of Aeronautics and Astronautics, Massachusetts Institute of Technology, Cambridge, 1991.

[14] N. M. Wereley and S. R. Hall, "Linear time periodic systems: transfer functions, poles, transmission zeroes and directional properties," presented at the Proceedings of the 1991 American Control Conference, Boston, MA, USA, 1991.

[15] N. M. Wereley and S. R. Hall, "Frequency response of linear time periodic systems," Honolulu, HI, USA, 1990, pp. 3650-3655.

[16] C. P. Ratcliffe, "A Frequency and Curvature Based Experimental Method for Locating Damage in Structures," *Journal of Vibration and Acoustics,* vol. 122, pp. 324-328, 2000.

[17] V. K. Sharma, S. Hanagud, and M. Ruzzene, "Damage index estimation in beams and plates using laser vibrometry," *AIAA Journal,* vol. 44, pp. 919-23, 2006.

[18] N. M. Wereley, "Analysis and Control of Linear Periodically Time Varying Systems," PhD, Department of Aeronautics and Astronautics, Massachusetts Institute of Technology, Cambridge, 1991.

[19] C.-T. Chen, *Linear system theory and design*, 3rd edtion ed.: Oxford University Press, Inc, 1999.

[20] P. Martin and S. Rothberg, "Introducing speckle noise maps for laser vibrometry," *Optics and Lasers in Engineering,* vol. 47, pp. 431-42, 2009.

[21] S. J. Rothberg, "Laser vibrometry. Pseudo-vibrations," *Journal of Sound and Vibration,* vol. 135, pp. 516-522, 1989.

[22] S. J. Rothberg and B. J. Halkon, "Laser vibrometry meets laser speckle," Ancona, Italy, 2004.

[23] S. Rothberg, "Numerical simulation of speckle noise in laser vibrometry," *Applied Optics,* vol. 45, pp. 4523-33, 2006.

[24] M. Martarelli and D. J. Ewins, "Continuous scanning laser Doppler vibrometry and speckle noise occurrence," *Mechanical Systems and Signal Processing,* vol. 20, pp. 2277-89, 2006.

[25] M. W. Sracic and M. S. Allen, "Experimental Investigation of the Effect of Speckle Noise on Continuous Scan Laser Doppler Vibrometer Measurements," presented at the 27th International Modal Analysis Conference (IMAC XXVII), Orlando, Florida, 2009.

[26] M. S. Allen and J. H. Ginsberg, "A Global, Single-Input-Multi-Output (SIMO) Implementation of The Algorithm of Mode Isolation and Applications to Analytical and Experimental Data," *Mechanical Systems and Signal Processing,* vol. 20, pp. 1090–1111, 2006.

[27] P. Martin and S. Rothberg, "Laser Vibrometry and the secret life of speckle patterns," in *Eigth Int. Conf. on Vibration Measurements by Laser Techniques: Advances and Applications*, 2008.

[28] M. S. Allen, "Global and Multi-Input-Multi-Output (MIMO) Extensions of the Algorithm of Mode Isolation (AMI)," Doctorate, George W. Woodruff School of Mechanical Engineering, Georgia Institute of Technology, Atlanta, Georgia, 2005.

[29] G. Floquet, "Sur Les Equations Lineairs a Coefficients Periodiques," *Ann. Sci. Ecole Norm. Sup.,* vol. 12, pp. 47-88, 1883.

[30] C. Chen, *Linear Systems Theory and Design*, 3 ed. New York: Oxford University Press, Inc., 1999.

[31] J. Guckenheimer and P. Holmes, *Nonlinear Oscillations, Dynamical Systems, and Bifurcations of Vector Fields* vol. 42. New York: Springer-Verlag New York Inc., 1983.

[32] P. Hartman, *Ordinary Differential Equations*. New York: John Wiley & Sons, Inc., 1964.

[33] M. S. Allen, "Floquet Experimental Modal Analysis for System Identification of Linear Time-Periodic Systems," presented at the ASME 2007 International Design Engineering Technical Conference, Las Vegas, NV, 2007.

Appendix

The derivation of harmonic transfer function starts with the output expression of a linear system with time varying coefficients. The output *y*(*t*) of a general linear state space model can be found in [19] as follows,

$$y(t) = C(t)\Phi(t,t_0)x(t_0) + \int_{t_0}^{t} C(t)\Phi(t,\tau)B\left(\tau\right)u(\tau)d\tau + D(t)u(t) \tag{28}$$

where *u*(*t*) is the excitation or the input to the system, and *B*(*t*) is the input matrix that describes how the input is applied. *C*(*t*) is the output matrix that defines the output state, and *D*(*t*) is the direct input matrix to the output. $\Phi(t,t_0)$ is called the state transition matrix. It relates the system state *x*(*t*) at any time to the initial state $x(t_0)$ by,

$$x(t) = \Phi(t,t_0)x(t_0) \tag{29}$$

Finding the state transition matrix is the key to derive the harmonic transfer function. For a linear time invariant system with constant coefficients, the state transient matrix can be obtained directly as $\Phi(t,t_0) = e^{A(t-t_0)}$, where *A* is the system matrix of the state space model. However, this expression is not valid for a general time varying *A*(*t*). In this case, it is usually challenging or even impossible to find the closed form transient matrix.

Fortunately, for a system with periodic matrices, e.g. $A(t) = A(t+T_A)$ where $T_A = 2\pi / \omega_A$ is called the fundamental period, Floquet theorem [29-32] has defined a coordinate change of the state *x*(*t*) that transforms the periodic system to a time invariant system, such that linear time periodic systems can be studied using time invariant techniques. Following the Floquet theorem, the state transition matrix of a linear time periodic system can be decomposed into the following modal summation form [33],

$$\Phi(t,t_0) = \sum_{r=1}^{N} \psi_r(t) L_r^T(t_0) e^{\lambda_r(t-t_0)} \tag{30}$$

where $\psi_r(t)$ is the r^{th} time-periodic mode vector of the transition matrix, and $L_r(t)$ is the r^{th} column of $\Psi(t) = \begin{bmatrix}\psi_1(t) & \psi_2(t) & \cdots\end{bmatrix}^{-T}$. λ_r is the r^{th} Floquet exponent, which is analogous to the eigenvalue of an time invariant system. The Floquet exponent can be written in terms of the damping ratio ζ_r and natural frequency ω_r as $\lambda_r = -\zeta_r\omega_r + \mathrm{i}\omega_r\sqrt{1-\zeta_r^{\,2}}$ for an under-damped mode.

To define the input-output relationship of a periodic system, we also have to introduce the exponentially modulated signal. It is well known that a single frequency excitation to a linear time invariant system, e.g. a linear oscillator, will cause the output at the same frequency though with different amplitude and phase. On the contrary, the response of a single frequency input to an asymmetric rotating rotor, a typical linear time periodic system, will be at the same frequency as well as its infinite number of harmonics, each separated by the fundamental frequency ω_A. Hence if we defined the input $u(t)$ and the output $y(t)$ of a linear time periodic system as the summation of frequency components separated by a multiple of the fundamental frequency ω_A,

$$u(t)=\sum_{n=-\infty}^{\infty} U_n e^{(\mathrm{i}\omega+\mathrm{i}n\omega_A)t} \quad , \quad y(t)=\sum_{n=-\infty}^{\infty} Y_n e^{(\mathrm{i}\omega+\mathrm{i}n\omega_A)t} \tag{31}$$

denoted by the exponentially modulated periodic input and output [13]. It is clear that a modulated input will cause a modulated output at the same collection of frequencies. So an input-output relationship that is completely analogous to time invariant transfer function can be established.

Wereley extended the concept of a transfer function for LTI systems to LTP systems using the Floquet theorem and the exponentially modulated periodic signal space defined above. First, the expression of the state transition matrix in Eq. (30) is substituted into the general solution of the state space model in Eq. (28), the general solution becomes,

$$\begin{aligned} y(t)=&\sum_{r=1}^{2N} C(t)\psi_r(t)e^{\lambda_r t}L_r^T(t_0)x(t_0)e^{-\lambda_r t_0} \\ &+\sum_{r=1}^{2N} C(t)\psi_r(t)e^{\lambda_r t}\int_{t_0}^{t} L_r^T(\tau)B(\tau)u(\tau)e^{-\lambda_r \tau}d\tau + D(t)u(t) \end{aligned} \tag{32}$$

Since the eigenvectors $\psi_r(t)$ of the state transition matrix are periodic, it is convenient to expand them into a Fourier series. As is often the case for time invariant systems, the output matrix $C(t)$ may simply be a matrix of ones and zeros indicating which of the states are being taken. In any event, the expansion is,

$$C(t)\psi_r(t)=\sum_{n=-\infty}^{\infty} \bar{C}_{r,n}e^{\mathrm{i}n\omega_A t} \quad , \quad L_r^T(t)B(t)=\sum_{n=-\infty}^{\infty} \bar{B}_{r,n}e^{\mathrm{i}n\omega_A t} \tag{33}$$

where $\bar{C}_{r,n}$ is the nth Fourier coefficient of the r^{th} observed mode vector, $C(t)\psi_r(t)$, and similarly for $L_r^T(t)B(t)$.

The harmonic transfer function can be derived by substituting the expression of exponentially modulated signals in Eq. (31), and the Fourier expansion in Eq. (33) into Eq. (32).

When studying the transfer function, only the steady state response is considered. Hence if we neglect the transient response, after much algebra, the output expression becomes,

$$\begin{aligned} \sum_{n=-\infty}^{\infty} Y_n e^{(\mathrm{i}\omega+\mathrm{i}n\omega_A)t} =&\sum_{r=1}^{2N}\sum_{n=-\infty}^{\infty}\sum_{s=-\infty}^{\infty}\sum_{m=-\infty}^{\infty} \frac{\bar{C}_{r,s}\bar{B}_{r,m}}{\mathrm{i}\omega-\lambda_r+\mathrm{i}(m+n)\omega_A} U_n e^{(\mathrm{i}\omega+\mathrm{i}(n+s+m)\omega_A)t} \\ &+\sum_{n=-\infty}^{\infty} D(t)U_n e^{(\mathrm{i}\omega+\mathrm{i}n\omega_A)t} \end{aligned} \tag{34}$$

Now we introduce the exponentially modulated input and output in the frequency domain as follows,

$$\begin{aligned}\mathbf{U}(\omega) &= \begin{bmatrix}\cdots & U_{-1}(\omega)^T & U_0(\omega)^T & U_1(\omega)^T & \cdots\end{bmatrix}^{\mathrm{T}} \\ \mathbf{Y}(\omega) &= \begin{bmatrix}\cdots & Y_{-1}(\omega)^T & Y_0(\omega)^T & Y_1(\omega)^T & \cdots\end{bmatrix}^{\mathrm{T}}\end{aligned} \tag{35}$$

Using the harmonics balance approach, a transfer function can then be established in terms of the modal parameters of the state transition matrix, denoted by the harmonic transfer function.

$$\mathbf{Y}(\omega) = \mathbf{G}(\omega)\mathbf{U}(\omega) \tag{36}$$

Where,

$$\begin{aligned}\mathbf{G}(\omega) &= \sum_{r=1}^{2N}\sum_{l=-\infty}^{\infty}\frac{\overline{\mathbf{C}}_{r,l}\overline{\mathbf{B}}_{r,l}}{\mathrm{i}\omega-(\lambda_r-\mathrm{i}l\omega_A)}+\mathbf{D} \\ \overline{\mathbf{C}}_{r,l} &= \begin{bmatrix}\cdots & \overline{C}_{r,-1-l}{}^T & \overline{C}_{r,-l}{}^T & \overline{C}_{r,1-l}{}^T & \cdots\end{bmatrix}^T \\ \overline{\mathbf{B}}_{r,l} &= \begin{bmatrix}\cdots & \overline{B}_{r,l+1} & \overline{B}_{r,l} & \overline{B}_{r,l-1} & \cdots\end{bmatrix}\end{aligned} \tag{37}$$

Here the n^{th} term in the vector $\overline{\mathbf{C}}_{r,l}$, is $\overline{C}_{r,n-l}$, the $(n\text{-}l)^{\mathrm{th}}$ Fourier coefficient of $C(t)\psi_r(t)$. Similarly, $\overline{B}_{r,l-m}$ is the $(l\text{-}m)^{\mathrm{th}}$ Fourier coefficient of $L_r(t)^{\mathrm{T}}B(t)$. D is an infinite matrix with $D(t)$ on the diagonal.

This expression of harmonic transfer function has exactly the same mathematical form as the expression for the frequency response function of a linear time invariant system in terms of its modal parameters, so the same algorithms can be applied to identify the parameters of the linear time periodic system and the same intuition that one uses to interpret frequency response function can also be used to interpret harmonic transfer function. However, there are a few differences that must be noted:

- A linear time periodic system potentially has an infinite number of peaks for each mode in its harmonic transfer function. Each peak will occur near the imaginary part of the Floquet exponent λ_r plus some integer multiple of the fundamental frequency ω_A. If the mode shapes of the system are constant in time, then $\overline{\mathbf{C}}_{r,l}$ and $\overline{\mathbf{B}}_{r,l}$ contain only one nonzero term and Eq. (37) reduces to the familiar relationship for a linear time invariant system.
- The mode vectors of a linear time invariant system describe the spatial pattern of deformation of a mode. Each element in the mode vector indicates the physical deflection at the corresponding measurement point. For a linear time periodic system, the vectors $\overline{\mathbf{C}}_{r,l}$ consist of the Fourier coefficients that describe the time varying spatial deformation pattern.